Numerical Simulations of Heat Transfer in Taylor-Couette Flow

R. Kedia

M. L. Hunt
hunt@cco.caltech.edu

T. Colonius

Department of Engineering and Applied Science, California Institute of Technology, Pasadena, CA 91125

Numerical simulations have been performed to study the effects of the gravitational and the centrifugal potentials on the stability of heated, incompressible Taylor-Couette flow. The flow is confined between two differentially heated, concentric cylinders, and the inner cylinder is allowed to rotate. The Navier-Stokes equations and the coupled energy equation are solved using a spectral method. To validate the code, comparisons are made with existing linear stability analysis and with experiments. The code is used to calculate the local and average heat transfer coefficients for a fixed Reynolds number (Re = 100) and a range of Grashof numbers. The investigation is primarily restricted to radius ratios 0.5 and 0.7 for fluids with Prandtl number of about 0.7. The variation of the local coefficients of heat transfer on the cylinder surface is investigated, and maps showing different stable states of the flow are presented. Results are also presented in terms of the equivalent conductivity, and show that heat transfer decreases with Grashof number in axisymmetric Taylor vortex flow regime, and increases with Grashof number after the flow becomes nonaxisymmetric.

Introduction

Since the publication of the classic experimental and analytical paper by Taylor (1923), numerous studies on the transitions in circular Couette flow have been made. The flow undergoes a series of transitions (Coles, 1965; Brandstater and Swinney, 1987) before it becomes fully turbulent at very high rotational rates of the inner cylinder. The flow becomes even more complex if either radial heating or superimposed axial flow (Shih and Hunt, 1992) are present or if the cylinders are eccentrically oriented. The effects of a radial temperature gradient on the stability of Taylor-Couette flows has been the subject of considerable investigation (Ali and Weidman, 1990; Chen and Kuo, 1990). The primary application of this research is in the cooling of electrical motor shafts and turbine rotors (Lee and Minkowycz, 1989). Other applications include modeling of atmospheric flows (Greenspan, 1968) and techniques of chemical vapor deposition (CVD) used in semiconductor device fabrication (Singer, 1984).

In Boiling Water Reactor (BWR) power plants, high speed pumps are used to transport water at high pressure and temperature. Over the past decade, maintenance inspections have revealed cracks up to 6 mm deep on both the shafts and the shaft covers of such pumps; these cracks arise after approximately 20,000 to 30,000 hours of operation (Kato et al., 1992; Gopalakrishnan et al., 1992). In extreme instances, these cracks actually cause pumps to fail. The manufacturers and operators of the pumps have surmised that the cracking is due to thermal loading caused by an unsteady flow. Some preliminary work in this area has shown that these cracks could be initiated by low-frequency, high-amplitude temperature fluctuations. To predict thermal fatigue in these pumps, a thermal stress analysis would require information about the frequencies and amplitudes of the thermal environment. A focus of this work is to obtain such frequency and amplitude information for the model.

Previous investigations of heated Taylor-Couette flows include theory, experiment, and numerical analysis. There are a number of parameters in this problem; among them are the Reynolds number ($\mathrm{Re} = \omega r_i b/\nu$) and the Grashof number ($\mathrm{Gr} = g\beta(T_1 - T_2)b^3/\nu^2$). Typically in an experiment, the Reynolds number is increased by increasing the angular velocity of the inner cylinder, and the Grashof number is increased by increasing the temperature difference between the inner and the outer cylinders. As these two parameters are varied, the flow changes from one state to another, and there is a subsequent change in momentum and heat transfer characteristics. There is a need to understand these transitions and document the transport properties.

Theoretical investigations include stability analyses for these flows. For high Reynolds number, previous work in this area neglected gravity and showed that the Taylor cells are stabilized when $T_1 > T_2$ and destabilized when $T_2 > T_1$. Roesner (1978) included the effect of gravity through the Boussinesq approximation (Gray and Giorgini, 1976) but only considered axisymmetric disturbances. This work showed that isothermal Taylor cells are stabilized by both negative and positive radial heating, and the stability boundaries revealed perfect symmetry with respect to the direction of radial heating. Ali and Weidman (1990) tested stability with respect to both toroidal and helical disturbances of uniform wavenumber. They found that the number of critical modes increased dramatically for large radius ratio. Chen and Kuo (1990) took into account the effects of both centrifugal and gravitational potential on the axisymmetric stability problem. They concluded that the stability boundary depended on the ratio of the centrifugal and the gravitational potentials, the Prandtl number, and the Grashof number.

An experimental study was performed by Kataoka et al. (1977) with the aid of an electrochemical technique under the assumption of analogy between heat and mass transfer. They reported that the regular sinusoidal variation of Sherwood number (Sh) is distorted by an added axial flow and both the mean and the amplitude are greatly reduced. Ball and co-workers (1989) performed a parametric study of the mean heat transfer rates across the annular gap for three different radius ratios. Their results show that the heat transfer can be described by a power-law relationship and correlated as functions of the Reynolds number and radius ratio.

Numerical simulations for axisymmetric, isothermal Taylor-Couette flow have been performed by Meyer (1967), using a finite difference technique. Moser et al. (1983) used a spectral method for solving the incompressible Navier-Stokes equations between concentric cylinders. In the present study, their method is extended to solve both the heat equation and the equations

Contributed by the Heat Transfer Division for publication in the JOURNAL OF HEAT TRANSFER and presented at '97 NHTC, Baltimore. Manuscript received by the Heat Transfer Division April 11, 1997; revision received October 23, 1997; Keywords: Flow Instability; Numerical Methods; Rotating Flows. Associate Technical Editor: R. W. Douglass.

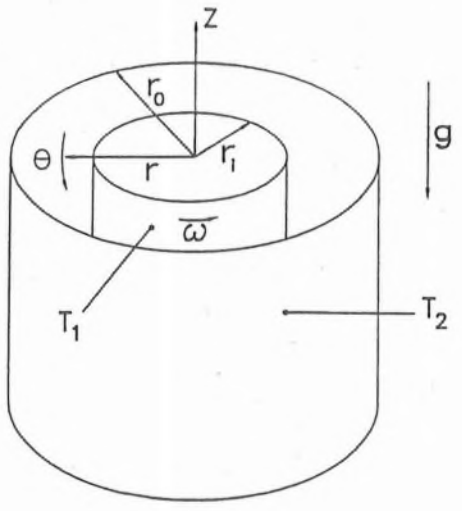

Fig. 1 Flow geometry and boundary conditions

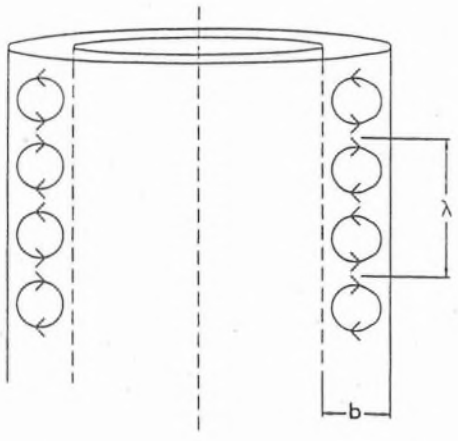

Fig. 2 Schematic of isothermal Taylor cells

of motion, which are coupled through the centrifugal and gravitational potentials. The effects of buoyancy on bifurcation in small-to-moderate aspect ratio Taylor-Couette systems have been studied numerically by Ball and Farouk (1987, 1988).

When the centrifugal acceleration is of the same order as the acceleration due to gravity, the density variation of the fluid becomes important for instabilities that are primarily centrifugal. The effect of this density variation is also accounted for in the centrifugal term. Therefore, the present study examines the interaction of gravity and centrifugal potentials with the radial temperature gradient. The simulations reported here are motivated by the need to characterize the thermal environment that is encountered during chaotic and fully turbulent flows.

Numerical Method

A sketch of the flow configuration in (r, θ, z) cylindrical coordinates is shown in Fig. 1. The radii of the inner and the outer cylinders are r_i and r_o, respectively, and the radius ratio is η. The inner cylinder rotates with a constant angular velocity ω about the vertical z-axis, while the outer cylinder is stationary. The two cylinders are at different uniform temperatures. The temperature of the inner cylinder is T_1 and that of the outer one is T_2. Gravity acts in the negative z-direction. The centrifugal force is parallel to the mean temperature gradient. The temperature difference can be assumed to be sufficiently small such that the density is treated as a constant everywhere in the Navier-Stokes equations with the exception of the gravitational (z-momentum equation) and the centrifugal (r-momentum equation) terms, i.e., the Boussinesq approximation is applied. All other fluid properties are assumed to be independent of temperature. The flow is axially periodic (i.e., infinite aspect ratio) and no slip boundary conditions are used at the inner and the outer cylinders. Figure 2 shows schematically the familiar axisymmetric counter-rotating isothermal Taylor cells. Without heating, the Taylor cells are of uniform size. The axial distance between a pair of Taylor cells is defined as axial wavelength (λ) and b is the gap width. The axial wavelength is normalized by the gap width to define L_z.

Nomenclature

A = acceleration ratio, $\omega^2 r_i/g$
b = gap width, $(r_o - r_i)$ [m]
C = Courant number
C_b = bulk concentration [mol/m^3]
C_w = concentration at the outer cylinder surface [mol/m^3]
c = nondimensional wave speed
D = mass diffusivity of the fluid [m^2/s]
f = frequency of heat transfer coefficient fluctuation [1/s]
f_c = inner cylinder frequency [1/s]
G = torque [N − m]
Gr = Grashof number, $g\beta(T_1 - T_2)b^3/\nu^2$
g = acceleration due to gravity [m/s^2]
h = local heat transfer coefficient, $q/(T_b - T_2)$ [W/m^{2}K]
$h_{\theta,zt}$ = spatially and temporally averaged heat transfer coefficient [W/m^{2}K]
K_{eq} = mean equivalent conductivity, $r_i \ln(1/\eta) h_{\theta,zt}/k$
k = thermal conductivity of the fluid [W/mK]
L_z = normalized axial wavelength, λ/b
m = local mass transfer coefficient, $N/(C_b - C_w)$ [m/s]
N = mass flux on the outer cylinder [mol/m^{2}s]
Nu = Nusselt number, $2hb/k$
n = number of starts, $2\pi r_o \tan \Psi/L_z$
P = nondimensional dynamic pressure
Pr = Prandtl number, ν/α
q = heat flux on the outer cylinder
Re = Reynolds number, $\omega r_i b/\nu$
Re_{crit} = critical Reynolds number for the onset of Taylor vortex flow
r, θ, z = cylindrical coordinates
r_i = inner cylinder radius [m]
r_o = outer cylinder radius [m]
Sc = Schmidt number, ν/D
Sh = Sherwood number, $2mb/D$
T = nondimensional temperature
T_1 = inner cylinder temperature [K]
T_2 = outer cylinder temperature [K]
T_b = bulk temperature [K]
T_o = dimensionless reference temperature
u_r, u_θ, u_z = nondimensional velocity component in cylindrical coordinate system
ω = inner cylinder angular velocity [1/s]
ρ = density of the fluid [kg/m^3]
ν = kinematic viscosity of the fluid [m^2/s]
α = thermal diffusivity of the fluid [m^2/s]
β = thermal expansion coefficient of the fluid [1/K]
β^* = $\beta(T_1 - T_2)$
λ = wavelength of a pair of vortices [m]
η = radius ratio, r_i/r_o
Ψ = the angle of inclination of the cell from the horizontal
Δt = nondimensional time step of integration
$\Delta r, \Delta\theta, \Delta z$ = grid spacing in the radial, circumferential, and axial directions

The equations are made dimensionless by scaling lengths with b, time with $b/\omega r_i$, velocity with ωr_i, and temperature with $(T_1 - T_2)$, after subtracting the outer cylinder temperature and dynamic pressure with $\omega^2 r_i^2$. The nondimensional equations governing the flow for the nondimensional velocity components (u_r, u_θ, u_z), nondimensional dynamic pressure P and nondimensional temperature T (in rotational form) follow.

Continuity.

$$\frac{\partial u_r}{\partial r} + \frac{u_r}{r} + \frac{1}{r}\frac{\partial u_\theta}{\partial \theta} + \frac{\partial u_z}{\partial z} = 0 \tag{1}$$

Momentum.

$$\frac{\partial u_r}{\partial t} + \frac{u_\theta}{r}\frac{\partial u_r}{\partial \theta} + u_z\frac{\partial u_r}{\partial z} - u_z\frac{\partial u_z}{\partial r} - u_\theta\frac{\partial u_\theta}{\partial r} - (1 - \beta^*(T - \overline{T_o}))\frac{u_\theta^2}{r} = -\frac{\partial P}{\partial r} + \frac{1}{\mathrm{Re}}\left(\frac{1}{r^2}\frac{\partial^2 u_r}{\partial \theta^2} - \frac{1}{r^2}\frac{\partial u_\theta}{\partial \theta} - \frac{1}{r}\frac{\partial^2 u_\theta}{\partial \theta \partial r} + \frac{\partial^2 u_r}{\partial z^2} - \frac{\partial^2 u_z}{\partial r \partial z}\right) \tag{2}$$

$$\frac{\partial u_\theta}{\partial t} + \frac{u_r u_\theta}{r} + u_r\frac{\partial u_\theta}{\partial r} - \frac{u_r}{r}\frac{\partial u_r}{\partial \theta} - \frac{u_z}{r}\frac{\partial u_z}{\partial \theta} + u_z\frac{\partial u_\theta}{\partial z} = -\frac{1}{r}\frac{\partial P}{\partial \theta} + \frac{1}{\mathrm{Re}}\left(\frac{1}{r}\frac{\partial u_\theta}{\partial r} - \frac{u_\theta}{r^2} + \frac{\partial^2 u_\theta}{\partial r^2} + \frac{1}{r^2}\frac{\partial u_r}{\partial \theta} - \frac{1}{r}\frac{\partial^2 u_r}{\partial r \partial \theta} - \frac{1}{r}\frac{\partial^2 u_z}{\partial z \partial \theta} + \frac{\partial^2 u_\theta}{\partial z^2}\right) \tag{3}$$

$$\frac{\partial u_z}{\partial t} - u_r\frac{\partial u_r}{\partial z} + u_r\frac{\partial u_z}{\partial r} + \frac{u_\theta}{r}\frac{\partial u_z}{\partial \theta} - u_\theta\frac{\partial u_\theta}{\partial z} = -\frac{\partial P}{\partial z} + \frac{1}{\mathrm{Re}}\left(\frac{1}{r}\frac{\partial u_z}{\partial r} - \frac{1}{r}\frac{\partial u_r}{\partial z} - \frac{\partial^2 u_r}{\partial r \partial z} + \frac{\partial^2 u_z}{\partial r^2} + \frac{1}{r^2}\frac{\partial^2 u_z}{\partial \theta^2} - \frac{1}{r}\frac{\partial^2 u_\theta}{\partial z \partial \theta}\right) + \frac{\mathrm{Gr}}{\mathrm{Re}^2}(T - \overline{T_o}) \tag{4}$$

with $(u_r, u_\theta, u_z) = (0, 1, 0)$

at the nondimensional inner radius, $\eta/(1 - \eta)$

and $(u_r, u_\theta, u_z) = (0, 0, 0)$

at the nondimensional outer radius, $1/(1 - \eta)$

Energy.

$$\frac{\partial T}{\partial t} + u_r\frac{\partial T}{\partial r} + \frac{u_\theta}{r}\frac{\partial T}{\partial \theta} + u_z\frac{\partial T}{\partial z} = \frac{1}{\mathrm{Pr}\,\mathrm{Re}}\left(\frac{1}{r}\frac{\partial T}{\partial r} + \frac{\partial^2 T}{\partial r^2} + \frac{1}{r^2}\frac{\partial^2 T}{\partial \theta^2} + \frac{\partial^2 T}{\partial z^2}\right) \tag{5}$$

with $T = 1$ at the nondimensional inner radius, $\eta/(1 - \eta)$

and $T = 0$ at the nondimensional outer radius, $1/(1 - \eta)$

Geometric parameters include η and L_z. Another useful parameter is the acceleration ratio, $A = \omega^2 r_i/g$, which is the ratio of the centrifugal to gravitational accelerations. It can be derived from the independent parameters ($A = \mathrm{Re}^2\beta^*[1/\eta - 1]/\mathrm{Gr}$).

The three-dimensional incompressible equations of motion, together with the energy equation, are discretized using a Chebyshev/Fourier spectral method. Writing the solution V_s and T_s as a truncated series expansion, using trial functions as basis functions,

$$V_s(r, \theta, z, t) = \sum_{K_\theta}\sum_{K_z}\sum_{l=0}^{L}\alpha_{jml}(t)u_l(r; K_\theta, K_z)e^{iK_\theta\theta}e^{iK_z z} \tag{6}$$

$$T_s(r, \theta, z, t) = \sum_{K_\theta}\sum_{K_z}\sum_{l=0}^{L}\gamma_{jml}(t)\tau_l(r; K_\theta, K_z)e^{iK_\theta\theta}e^{iK_z z}, \tag{7}$$

where K_z and K_θ are the wave numbers, and L is the number of modes in the r-direction. The expansion coefficients are given by $\alpha_{jml}(t)$ and $\gamma_{jml}(t)$; $u_l(r; K_\theta, K_z)$ and $\tau_l(r; K_\theta, K_z)$ are the r-trial functions for the velocity and the temperature fields. This method uses spectral expansions that inherently satisfy the boundary conditions and Eq. (1) (Moser et al., 1983). Fourier series expansions are used in the z-direction and θ-direction, and modified Chebyshev polynomials are used in the r-direction. The equations of motion and the energy equation are coupled, but the method yields banded matrices, which can be efficiently solved at each time step. The viscous term is treated implicitly (Crank-Nicholson), whereas an explicit (Adams-Bashforth) scheme is used for the convective terms. The nonlinear terms act as a forcing term to the implicit part of the calculation and are computed using the pseudospectral (collocation) technique on a grid dense enough to eliminate aliasing by the 3/2 rule (Canuto et al., 1988). The calculations were performed using 32 Fourier modes each in z and θ-directions and Chebyshev polynomials through thirty-first degree in the r-direction. A nondimensional time step (Δt) of 0.05 was used in all the computations, which yielded a maximum Courant number of 0.75, where the Courant number C is defined as

$$C = \pi\Delta t\left(\left|\frac{u_r}{\Delta r}\right| + \left|\frac{u_\theta}{r\Delta\theta}\right| + \left|\frac{u_z}{\Delta z}\right|\right). \tag{8}$$

To establish convergence, a series of higher resolution simulations (64^3) with a smaller time step were performed. The three components of velocity and the temperature were monitored at the same physical location as for the coarser resolution. The two gave an identical time trace which proved the adequacy of the coarser (32^3) simulation. Full details of the numerical scheme are given in Kedia (1997).

Results and Discussion

Comparison With Linear Stability Theory. The accuracy of the code was checked by comparing it with a linear stability analysis (Chen et al., 1990) for $\eta = 0.9$, $L_z = 2.007$, and $\mathrm{Pr} = 0.71$. Chen and Kuo (1990) investigated the interaction of a radial temperature gradient with both gravity and centrifugal potentials. Their linear stability analysis showed that the critical Reynolds number depended on the ratio of the centrifugal and gravitational potentials, the Prandtl number, and the Grashof number. The results are summarized in Table I. Case (1) and (2) refer to constant density simulations ($\beta^* = 0$) and case (3) and (4) refer to simulations where density is allowed to depend on temperature. To check for the critical Reynolds number, perturbations are introduced in the simulation. If the perturbations decay in time (with the flow returning to the steady base flow), then the flow is stable. Otherwise, the flow is unstable. The error margin for critical Reynolds number (case 1) indicates that the disturbances died down for $\mathrm{Re} = 132.2$ and grew into Taylor cells for $\mathrm{Re} = 132.6$. The error margin for wave speed is based on the time step. The critical Reynolds number ($\mathrm{Re}_{\mathrm{crit}}$) for the onset of Taylor cells, and the computed wave speed (c) agree very well with the linear stability theory.

Comparison With Experiments. The code is also compared with experimental results. One of the results from Kataoka et al. (1977) is replotted in Fig. 3 (symbols). In their experi-

Table 1 Comparison with linear stability theory

Case	Stability Analysis of Chen and Kuo (1990)	Simulation
η=0.9 L_z=2.007 Pr=0.71		
(1) Gr=200 β^*=0 Re_{crit}	132.39	132.4±0.2
c	0.00142	0.00142±0.00001
(2) Gr=-200 β^*=0 Re_{crit}	132.39	132.4±0.2
c	−0.00142	−0.00142±0.00001
(3) Gr=200 β^*=0.133 Re_{crit}	134.91	134.8±0.2
c	0.00130	0.00131±0.00001
(4) Gr=-200 β^*=-0.138 Re_{crit}	129.96	130.0±0.2
c	−0.00153	−0.00152±0.00001

ment, they measured the local coefficient of mass transfer on the outer cylinder. The Schmidt and Grashof numbers are not given in the paper, but are estimated to be of order 10^5 and 100, respectively (an approximate estimation was made from the range of values of ν, $CuSO_4$ molarity and wt% of Glycerin). The figure also shows (solid lines) the numerical results for the local Nusselt numbers obtained for the numerical simulation for the same η and L_z, but for Pr = 0.71. The axial wavelengths imposed in the simulation results shown in Fig. 3 are taken from the experiments of Kataoka et al. For Gr $\approx$ 100, the effect of natural convection is small, and the flow state remains axisymmetric; hence, in the heat transfer calculations, the Grashof number is taken to be zero. The local heat transfer coefficient is based on the temperature difference between the bulk of the fluid and the outer cylinder. The comparison between the mass transfer experiments and the heat transfer calculations show reasonable agreement. Some of the differences may be due to the assumption of Sc and Gr numbers. The simulations show that the adjacent Taylor cells are of equal size for Gr = 0. However, the relative size of Taylor cells varies with the increase in the differential heating of the two concentric cylinders. The slight difference in the relative size of Taylor cells is also seen in Fig. 3 from the experimental values of Kataoka et al. (1977). This difference is probably due to small Grashof number (based on mass transfer) effects. Note that the exponent has a value of 0.375, which was chosen to bring the results closer together. If the exponent is 0.333 (as used in the experiments), the values from the simulations were found to be smaller than the experimental values. The simulation can not be run for a very high Pr because the energy equation becomes stiff.

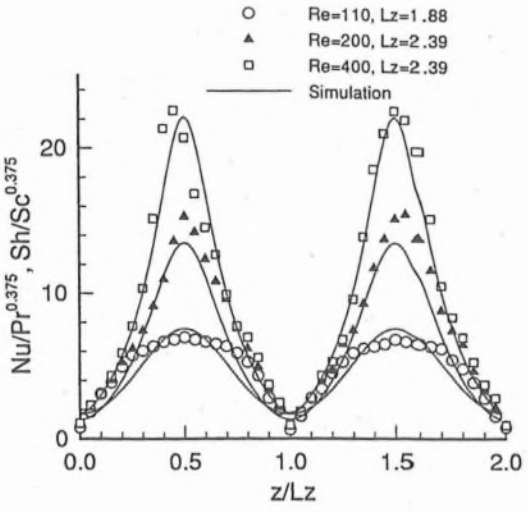

Fig. 3 Variation of heat (present simulation) and mass transfer (Kataoka et al., 1977) on the outer cylinder for η = 0.617

The second set of experiments used to validate the code is from the heat transfer experiments of Ball et al. (1989). In this experiment, the walls were maintained at uniform temperatures. The inner cylinder was heated by a cartridge heater and the outer cylinder was cooled by passing an ethylene glycol-water mixture through a flexible plastic hose coiled around it. The mean equivalent conductivity, K_{eq}, is defined as the ratio of the average convective heat transfer coefficient ($h_{\bar{a},\bar{c}T}$) to the heat transfer coefficient for pure conduction. The average convective heat transfer coefficient is based on the temperature difference between the inner and the outer cylinders. In Fig. 4, K_{eq} is plotted versus Re^2 for η = 0.565, L_z = 1.991, Gr = 1900, and

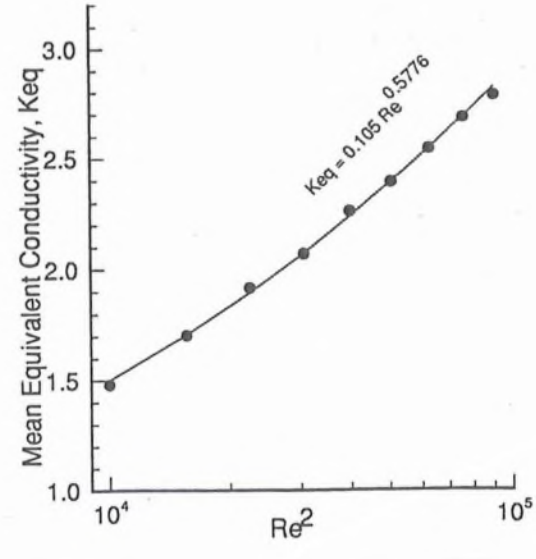

Fig. 4 Variation of heat transfer rate with Re^2 for η = 0.565, L_z = 1.991, Gr = 1900, and β^* = 0.053

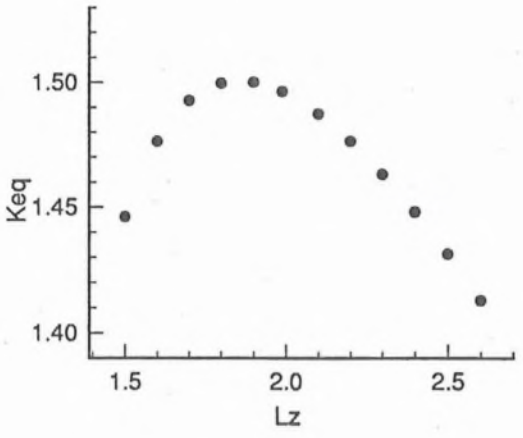

Fig. 5 Variation of mean equivalent conductivity with L_z for η = 0.5, Re = 100, Gr = 1700, and β^* = 0.0128

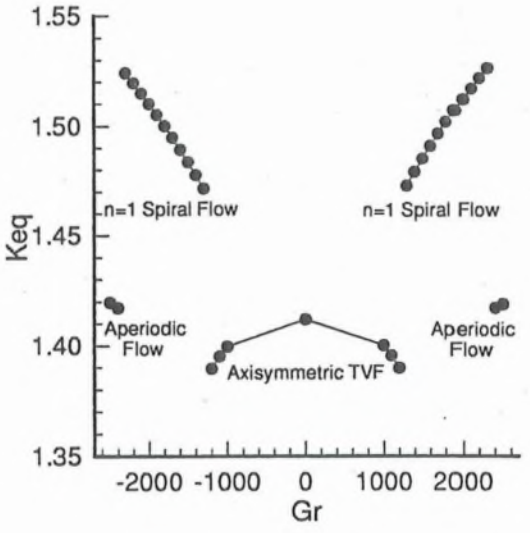

Fig. 6 Map showing different stable states present in the flow for η = 0.5, L_z = 1.988, Re = 100, Pr = 0.7, and A = 0.1285

$\beta^* = 0.053$. The normalized wavelength of approximately 1.991 is the critical wavelength corresponding to the critical Reynolds number for a radius ratio of 0.565, as given by the linear stability analysis. It is assumed that the axial wavelength remains fairly constant in the range of Reynolds number studied here, and this critical wavelength is chosen as the axial period of the flow. The result shows a power law behavior, which has a lower coefficient and a higher exponent than the result presented by Ball et al. This discrepancy arises because of the variation of axial wavelength with axial distance resulting from the thermal conditions at the ends of the experimental apparatus. The simplifying assumption of no axial temperature gradient could be another source of discrepancy between the experiment and the numerics. The simulations also show that for Gr = 1900, as the Reynolds number is varied, the relative size of the adjacent counter-rotating Taylor cells change. This agrees qualitatively with the flow visualization studies of Ball et al. (1989).

Figure 5 shows that the heat transfer results are very sensitive to the imposed axial wavelength. Plotted is the variation of the calculated K_{eq} with L_z. The same average heat transfer coefficient can be achieved by two different wavelengths, one below the isothermal critical value (L_z = 1.988), and the other above it. A similar result was shown by Meyer (1967) in numerical calculations of torque. The author concluded that the experimentally observed torque is somewhat lower than the numerical torque; it is speculated that the same is true for the heat transfer as well.

Flow States for Varying Gr. Apart from calculating the local and the average heat transfer coefficients, it is important to know how the flow evolves from one state to another as Gr is varied. Figure 6 presents a map of different stable states in the flow for a fixed Reynolds number and different Gr. The circular Couette flow was the base flow, and the steady-state conduction field was the base temperature field. A random disturbance of magnitude one percent of the velocity of the inner cylinder was introduced to the laminar state (circular Couette flow) and allowed to grow into Taylor vortices. Reynolds number was slowly increased (in steps of 5) to achieve the desired Reynolds number. The result with the lower Reynolds number was used as initial condition for the next higher Reynolds number. Once the desired Reynolds number was reached, another random disturbance of magnitude one percent of the temperature difference between the two cylinders was imposed on the temperature initial condition in order to trigger transitions. For low |Gr|, axisymmetric Taylor Vortex Flow (TVF) is the stable state. Outside this range, n = 1 stripes are formed. Figure 7 shows a schematic of spiral flows for n = 1 and n = 2. These spirals move an axial distance of nL_z for one rotation around the inner cylinder. The flow becomes aperiodic for higher Gr.

Similar stripes were also seen in the flow visualization experiments of Snyder and Karlsson (1964) and Ball et al. (1989). Stripes of larger inclination angle, up to n = 6, were observed by Snyder and co-workers for higher heating in a small annulus (η = 0.957). Higher spiral modes are formed for narrower gaps (Ali et al., 1990).

Increasing Gr decreases the heat transfer coefficient (K_{eq}) within the axisymmetric TVF regime. The increase in the axial velocity as a result of increasing Gr not only delays the onset of Taylor vortices but also causes a damping effect on the heat transfer. A similar effect of decreasing of the average Sherwood number by an added axial flow was also observed by Kataoka et al. The mean equivalent conductivity, K_{eq}, increases significantly with the formation of n = 1 spiral flow, and it continues to increase with Gr until the flow becomes aperiodic with a subsequent decrease in K_{eq} near Gr = ±2400. The map is nearly symmetric about the Gr = 0 axis.

A similar map is shown for η = 0.7 in Fig. 8. Again, axisymmetric Taylor vortex flow is seen for low |Gr|, but the n = 1 spiral flow is formed for a broader negative range of Gr and for a narrower positive Gr. The n = 2 spiral flow is formed for higher negative Gr, and is not formed for positive Gr. The flow becomes aperiodic outside this range. The heat transfer has similar effects as for η = 0.5 (Fig. 6) in the TVF regime. However, instead of K_{eq} increasing monotonically in the n = 1 spiral flow regime, it attains a maximum for both positive and

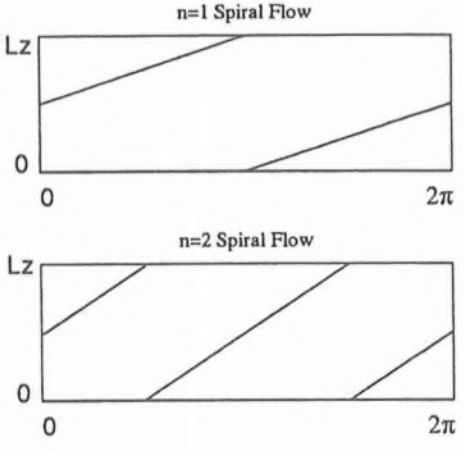

Fig. 7 Schematic of spiral flows

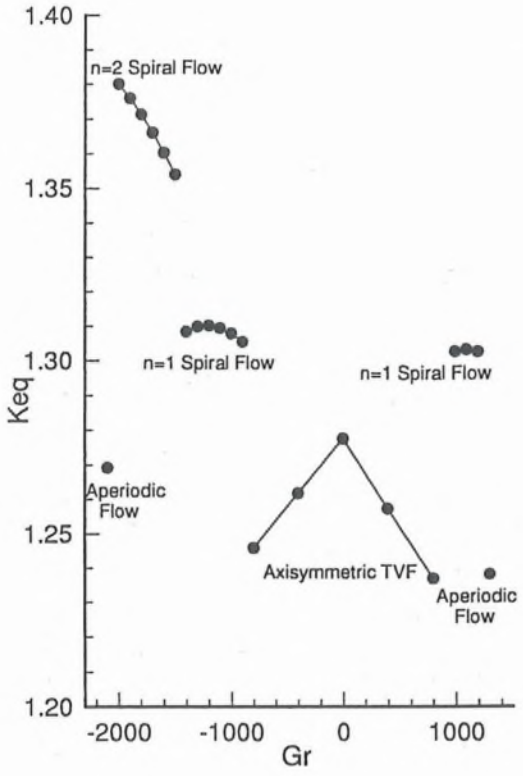

Fig. 8 Map showing different stable states present in the flow for η = 0.7, L_z = 2.001, Re = 100, Pr = 0.7, and A = 0.67

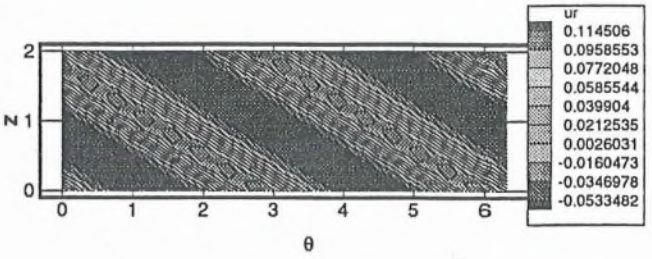

Fig. 10 Radial velocity contours at the mid radial section of the two cylinders for η = 0.7, L_z = 2.001, Re = 100, Pr = 0.7, and Gr = −1700

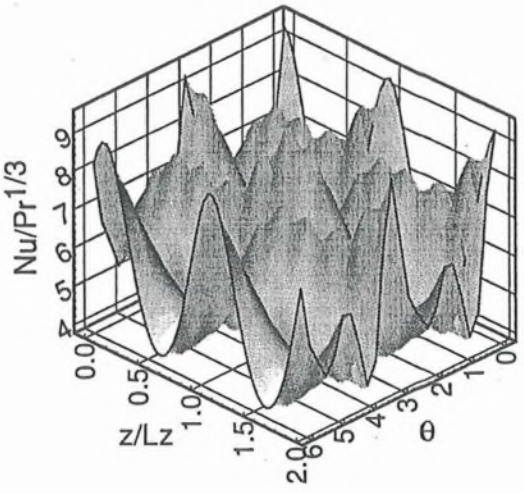

Fig. 11 Variation of heat transfer on the outer cylinder for η = 0.7, L_z = 2.001, Re = 100, Pr = 0.7, and Gr = −2100

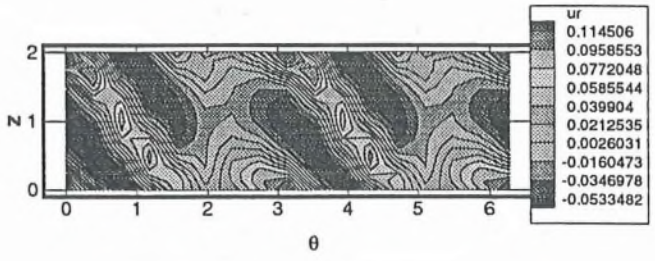

Fig. 12 Radial velocity contours at the mid-radial section of the two cylinders for η = 0.7, L_z = 2.001, Re = 100, Pr = 0.7, and Gr = −2100

negative Grashof numbers. A significant increase in K_{eq} is observed with the formation of n = 2 spiral flow, and K_{eq} increases with further increase in Gr in this regime of flow. This map is not symmetrical about the Gr = 0 axis. The asymmetry grows with the increase in the value of A. The onset of spirals correlate with both $|\mathrm{Gr}/\mathrm{Re}^2|$ and A. For higher A, the spirals start at lower $|\mathrm{Gr}/\mathrm{Re}^2|$.

The choice of L_z to determine the flow states (Figs. 6 and 8) was based on previously published linear stability analyses (DiPrima and Swinney, 1981). At the outset, it was unclear whether the flow states (n = 1 spiral, n = 2 spiral, or aperiodic) would be sensitive to the imposed axial wavelength, L_z. However, numerical experiments showed that the flow states were invariant as L_z was varied by as much as 50 percent, despite the fact that K_{eq} varied by as much as 6 percent (see Fig. 5). The results presented here are all based on the critical wavelength for L_z.

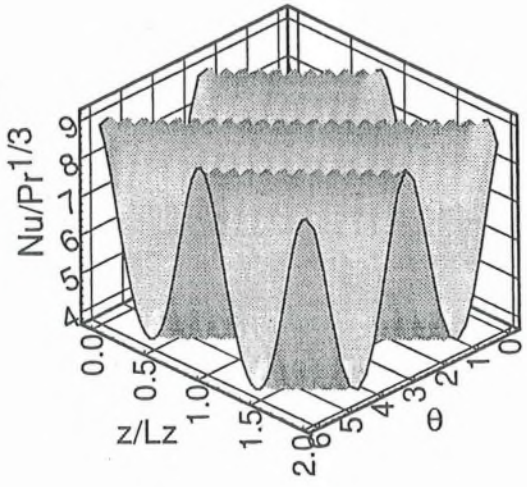

Fig. 9 Variation of heat transfer on the outer cylinder for η = 0.7, L_z = 2.001, Re = 100, Pr = 0.7, and Gr = −1700

The variation of heat transfer as a function of z and θ is shown in Fig. 9 (Gr = −1700, n = 2 spiral flow) and Fig. 11 (Gr = −2100, aperiodic flow). For Gr = −1700 the variation is sinusoidal in both z and θ. For Gr = −2100, the Nusselt number varies with z and θ in a more complicated way. The radial velocity contours corresponding to Figs. 9 and 11 are plotted in Figs. 10 and 12, respectively. For Gr = −1700 the two stripes are clearly evident, while for Gr = −2100 the flow is wavy and there is no single dominant frequency.

Finally, the frequencies and the amplitudes of local fluctuations of heat transfer coefficient (h) present in the flow are shown in Fig. 13. The frequency is normalized by the rotation frequency of the inner cylinder and the amplitude is normalized by the spatially and temporally averaged heat transfer coefficient. The figure shows that $f/f_c \simeq 0.35$ for n = 1 and the amplitude of local fluctuations of heat transfer is about 95 per-

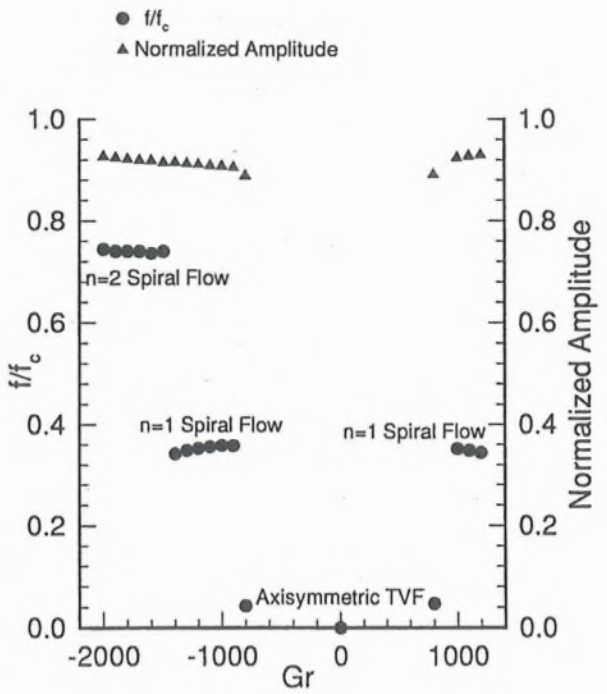

Fig. 13 Variation of frequency and amplitude with Grashof number for $\eta = 0.7$, $L_z = 2.001$, Re = 100, Pr = 0.7, and $A = 0.67$

cent of $h_{\bar{\theta},\tau f}$. The above information of the frequency and the amplitude of local fluctuations of heat transfer is required as boundary conditions for thermal stress analysis of the shaft and cover of BWR pumps. With the assumption that the frequency fluctuation is about 10 to 100 percent of rotating speeds, the predictive models (Gopalakrishnan et al., 1992) revealed crack depths which were comparable to field observations for the shaft and cover.

Conclusion

Heat transfer in an incompressible, three-dimensional Taylor-Couette flow with a rotating inner cylinder has been numerically investigated to study the interaction of gravity and centrifugal potentials with the radial temperature gradient. Calculation of critical Reynolds number and wave speed obtained from these simulations agree well with linear stability theory. For a certain range of Gr, the spatial variation of heat transfer on the inner and the outer cylinder is sinusoidal, and the magnitude of the Nusselt number increases with Reynolds number. The space and time averaged heat transfer from the inner to the outer cylinder is reported and is found to be sensitive to the imposed axial wavelength. The average heat transfer decreases with increased heating in the axisymmetric TVF regime. The equivalent conductivity increases significantly with the formation of higher order spirals. When the centrifugal acceleration becomes of the same order of magnitude as the acceleration due to gravity ($A \simeq 1$), higher mode spirals are formed when the outer cylinder is heated. Hence, the thermal environment present in the flow may be the cause for thermal stress fatigue in primary-loop recirculation pumps in BWR power plants. The results also show that when the flow is within the spiral flow regime (with either $n = 1$ or $n = 2$), the heat flux to the surface of the shaft is periodic with a period that is at frequencies of approximately 35 percent ($n = 1$) and 74 percent ($n = 2$) of the rotational frequency of the shaft. The local variation of the heat flux to the surface may be as much as 95 percent of the average.

Acknowledgments

This research was performed in part using the CSCC parallel computer system operated by Caltech on behalf of the Concurrent Supercomputing Consortium. Access to this facility was provided by Caltech. The authors would also like to thank Dr. A. Leonard at Caltech and Dr. R. D. Moser at University of Illinois at Urbana-Champagne for valuable discussions.

References

Ali, M., and Weidman, P. D., 1990, "On the Stability of Circular Couette Flow With Radial Heating," *J. Fluid Mech.*, Vol. 220, pp. 53–84.

Ball, K. S., and Farouk, B., 1987, "On the Development of Taylor Vortices in a Vertical Annulus With a Heated Rotating Inner Cylinder," *Int. J. Num. Meth. Fluids*, Vol. 7, pp. 857–867.

Ball, K. S., and Farouk, B., 1988, "Bifurcation Phenomena in Taylor-Couette Flow With Buoyancy Effects," *J. Fluid Mech.*, Vol. 197, pp. 479–501.

Ball, K. S., Farouk, B., and Dixit, V. C., 1989, "An Experimental Study of Heat Transfer in a Vertical Annulus With a Rotating Inner Cylinder," *Int. J. Heat Mass Transfer*, Vol. 32, No. 8, pp. 1517–1527.

Brandstater, A., and Swinney, H. L., 1987, "Strange Attractors in Weakly Turbulent Couette-Taylor Flow," *Phys. Rev. A*, Vol. 35, No. 5, pp. 2207–2220.

Canuto, C., Hussaini, M. Y., Quarteroni, A., and Zang, T. A., 1988, *Spectral Methods in Fluid Dynamics*, 3rd ed., Springer-Verlag, Berlin.

Chen, J., and Kuo, J., 1990, "The Linear Stability of Steady Circular Couette Flow With a Small Radial Temperature Gradient," *Phys. Fluids A*, Vol. 2, No. 9, pp. 1585–1591.

Coles, D., 1965, "Transition in Circular Couette Flow," *J. Fluid Mech.*, Vol. 21, pp. 385–425.

DiPrima, R. C., and Swinney, H. L., 1981, "Instabilities and Transition in Flow Between Concentric Rotating Cylinders," *Hydrodynamic Instabilities and the Transition to Turbulence*, H. L. Swinney and J. P. Gollub, eds., Springer-Verlag, Berlin, pp. 139–180.

Gopalakrishnan, S., Vaghasia, G. K., and Reimers, C. R., 1992, "Crack Propagation in Main Coolant Pumps," presented at Fifth Int. Workshop on Main Coolant Pumps, April 21–24, Orlando, FL.

Gray, D. D., and Giorgini, A., 1976, "The Validity of the Boussinesq Approximation for Liquids and Gases," *Int. J. Heat Mass Transfer*, Vol. 19, pp. 545–551.

Greenspan, H. P., 1968, *The Theory of Rotating Fluids*, Cambridge University Press, New York.

Kataoka, K., Doi, H., and Komai, T., 1977, "Heat/Mass Transfer in Taylor Vortex Flow With Constant Axial Flow Rates," *Int. J. Heat Mass Transfer*, Vol. 20, pp. 57–63.

Kato, H., Kanno, H., Hosokawa, M., Watanabe, A., Shitara, C., Ashizawa, K., Miyano, H., Narabayashi, T., Iikura, T., Hayashi, M., Endoh, A., and Takehara, H., 1992, "The Development of Advanced Nuclear Primary Loop Recirculating Pump (PLR Pump) for BWR Plant Considering Thermal Fatigue Problem," *Industrial and Environmental Applications of Fluid Mechanics*, Proc. of the ASME Winter Annual Meeting, FED-Vol 145, Sherif et al., eds., pp. 157–162.

Kedia, R., 1997, "An Investigation of Velocity and Temperature Fields in Taylor-Couette Flows," Ph.D. thesis, California Institute of Technology, Pasadena, CA.

Kreith, F., 1968, "Convection Heat Transfer in Rotating Systems," *Advances in Heat Transfer 5*, Academic Press, New York, pp. 129–251.

Lee, Y. N., and Minkowycz, W. J., 1989, "Heat Transfer Characteristics of the Annulus of Two-Coaxial Cylinders With One Cylinder Rotating," *Int. J. Heat Mass Transfer*, Vol. 32, pp. 711–722.

Meyer, K. A., 1967, "Time-Dependent Numerical Study of Taylor Vortex Flow," *Phys. Fluids*, Vol. 10, No. 9, pp. 1874–1879.

Moser, R. D., Moin, P., and Leonard, A., 1983, "A Spectral Numerical Method for the Navier-Stokes Equations With Applications to Taylor-Couette Flow," *J. Comput. Phys.*, Vol. 52, pp. 524–544.

Roesner, K. G., 1978, "Hydrodynamic Stability of Cylindrical Couette-Flow," *Arch. of Mech.*, Vol. 30, pp. 619–627.

Shih, A. C., and Hunt, M. L., 1992, "High-Taylor-Number Couette Flows With a Superposed Isothermal or Heated Axial Flow," *Proc. of the ASME National Heat Transfer Conf., General Papers in Heat Transfer*, HTD-Vol. 204, M. Jensen et al., eds. San Diego, CA.

Singer, H. P., 1984, "Techniques of Low Pressure Chemical Vapor Deposition," Semiconductor International, Denver, CO, May 1984, pp. 72–77.

Taylor, G. I., 1923, "Stability of a Viscous Liquid Contained Between Two Rotating Cylinders," *Phils. Trans. R. Soc. London*, Ser. A, Vol. 223, pp. 289–343.